Chapter 16
Dark Matter Searches at the CMS Experiment

Bhawna Gomber

Abstract The results are presented for the search for dark matter particles using data sample of proton-proton collisions at $\sqrt{s} = 13\,\text{TeV}$, collected with the CMS detector at the LHC and corresponding to an integrated luminosity of $35.9\,\text{fb}^{-1}$. Different final states with a mono-jet, mono-photon, and mono-Z signatures are considered, as well as processes with dark matter particles produced in association with a Higgs boson. The results are interpreted using the simplified models, which are then compared to the results from direct and indirect dark matter experiments.

16.1 Introduction

Several astrophysical observations [1] confirm the existence of dark matter (DM) in the universe. While, there is strong evidence for dark matter, at the moment direct observation of dark matter particles has not been confirmed. However, many theoretical models have been proposed in which DM and standard model (SM) particles interact with sufficient strength and produce DM with observable rates in high energy collisions at the CERN, LHC. In the scenario where DM would exist in the form of particles, cosmological observations strongly suggest it should be weakly interacting and massive. These Weakly Interacting Massive Particles (WIMPs) could be searched for with the CMS experiment at the CERN LHC.

The DM particles, if produced at the LHC, are not expected to leave an observable signal in the detector. However, if these particles recoil against an observable system of particles (X), they may produce a large transverse momentum imbalance (p_T^{miss}) in a collision event. This paper reviews some of the recent results for DM searches based on p_T^{miss}+X signature from the CMS experiment.

On behalf of the CMS collaboration, Supported by DST SERB.

B. Gomber (✉)
University of Hyderabad, Hyderabad, India
e-mail: bhawna.gomber@cern.ch

A. Giri and R. Mohanta (eds.), *Workshop on Frontiers in High Energy Physics 2019*, Springer Proceedings in Physics 248,
https://doi.org/10.1007/978-981-15-6292-1_16

The central feature of the CMS apparatus is a superconduction solenoid of 6 m internal diameter, providing a magnetic field of 3.8T. Within the solenoid volume are a silicon pixel and strip tracker, a lead tungstate crystal electromagnetic calorimeter, and a brass and scintillator hadron calorimeter, each composed of a barrel and two endcap sections. A more detailed description of the CMS detector can be found in [2].

Global event reconstruction follows the particle-flow (PF) algorithm [3], which aims to reconstruct and identify each individual particle in an event with an optimized combination of all subdetector information. The missing transverse momentum (p_T^{miss}) is defined as the negative vector sum of the transverse momenta of all PF candidates in an event.

16.2 Simplified Dark Matter Models

In simplified DM models, DM particles are assumed to be Dirac fermions that interact with SM particles through a spin-1 or spin-0 mediator [4]. These interactions are classified into four different types, depending on whether the mediator is a vector, axial-vector, scalar, or pseudoscalar particle. The spin-0 mediators are assumed to couple to the SM particles via Yukawa couplings. The SM Higgs boson is a specific example of a scalar mediator that may couple to the DM particles. There are 4 parameters of the Simplified Models: the dark matter mass (m_{DM}), the mediator mass (m_{med}), the strength of the coupling between mediator and SM quarks (g_q), and the strength of the coupling between the mediator and the DM particles (g_{DM}).

16.3 Monojet and Mono-V Hadronic

A search is presented for events resulting in final states with one or more energetic jets or a weak boson V which is either a W or Z boson decaying hadronically and an imbalance in p_T due to undetected particles resulting in 'monojet' and 'mono-V' final states, respectively, using data from proton-proton collisions at $\sqrt{s} = 13$ TeV corresponding to an integrated luminosity of 35.9 fb^{-1}.

Events are selected by requiring $p_T^{miss} > 200$ GeV and at least one AK4 jet jet p_T to be greater than 100 GeV in the central part of the detector $|\eta| < 2.5$. In addition events are required to have no isolated leptons, no isolated photons and no b-jets. The two categories are then distinguished by p_T and shape requirements on the jets. An event is considered to be in the mono-V category if the jet p_T is larger than 250 GeV, its invariant mass falls in the [65,105] GeV window and it has a N-subjettiness ratio τ_2/τ_1 smaller than 0.6. The N-subjettiness is a variable that catches

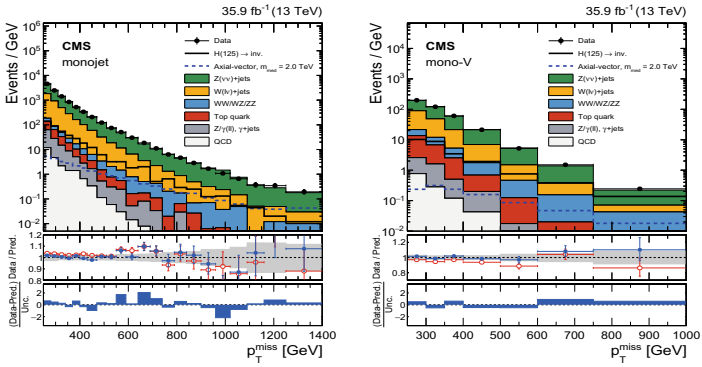

Fig. 16.1 Observed p_T^{miss} distribution in the monojet (left) and mono-V(right) signal regions compared with the post-fit background expectations for various SM processes. The last bin includes all events with $p_T^{miss} > 1250(750)$ GeV for the monojet (mono-V) category. The expected background distributions are evaluated after performing a combined fit to the data in all the control samples, not including the signal region. The fit is performed assuming the absence of any signal. Expected signal distributions for the 125 GeV Higgs boson decaying exclusively to invisible particles, and a 2 TeV axial-vector mediator decaying to 1 GeV DM particles, are overlaid. In the lower panels, ratios of data with the pre-fit background prediction (red open points) and post-fit background prediction (blue full points) are shown. The gray band in the lower panel indicates the post-fit uncertainty after combining all the systematic uncertainties. Finally, the distribution of the pulls, defined as the difference between data and the post-fit background prediction relative to the quadrature sum of the post-fit uncertainty in the prediction and statistical uncertainty in data, is shown in the lowest panel

the substructure of the jet. If the event fails the mono-V requirements, it is considered to be in the monojet category. The main backgrounds to the analysis are $Z(\nu\nu) + jets$ and $W + jets$ processes. The backgrounds are estimated using five control regions (CR) in data: dielectrons, dimuons and γ+jets (for $Z(\nu\nu)$) and single-electron and single-muon for $W + jets$.

The search is performed by extracting the signal through a combined fit of the signal and control regions. Figure 16.1 shows the p_T^{miss} distributions in the monojet and mono-V signal regions. The background prediction is obtained from a combined fit in all the control samples, excluding the signal region. Data are found to be consistent with the estimated background from the SM processes.

Upper limits are computed at 95% CL on the ratio of the measured signal cross section to the predicted one, with the CL s method [6], using the asymptotic approximation [7]. Limits are obtained as a function of the mediator mass and the DM mass. Figure 16.2 shows the exclusion contours in the m_{med} and m_{DM} plane for the vector and axial-vector mediators. Mediator masses up to 1.8 TeV, and DM masses up to 700 and 500 GeV are excluded for the vector and axial-vector models, respectively.

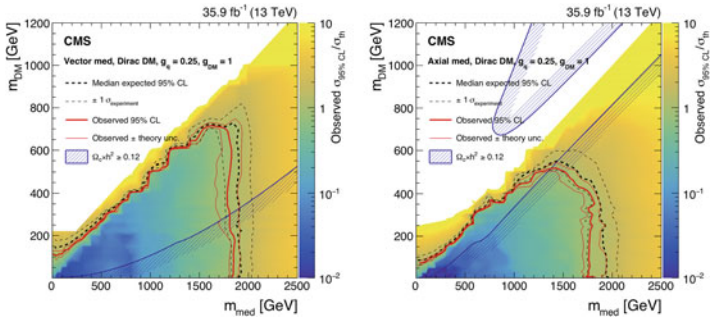

Fig. 16.2 Exclusion limits at 95% CL on μ in the m_{med} and m_{DM} plane assuming vector (left) and axial-vector (right) mediators. The solid (dotted) red (black) line shows the contour for the observed (expected) exclusion. The solid contours around the observed limit and the dashed contours around the expected limit represent one standard deviation due to theoretical uncertainties in the signal cross section and the combination of the statistical and experimental systematic uncertainties, respectively. Constraints from the Planck satellite experiment [5] are shown as dark blue contours; in the shaded area DM is overabundant

16.4 Monophoton and Mono-Z Search

The mono-photon search [8], target DM production in association with the initial state radiation of a high p_T photon. Similarly, a search is also performed in mono-Z final state, where Z bosond decays to electrons and muons. More details about mono-Z search can be found in [9].

In this search, events are selected with a high p_T photon with $p_T > 175\,\text{GeV}$ and $p_T^{miss} > 200\,\text{GeV}$. In addition events are required to have no isolated leptons, no jets. The main backgrounds to the analysis are $Z(\nu\nu) + \gamma$ and $W + \gamma$ processes. These backgrounds are estimated using four control regions (CR) in data: dielectrons, dimuons (for $Z(\nu\nu)$) and single-electron and single-muon for $W + \gamma$. This analysis also face major challenge from instrumental backgrounds i.e. spikes and beam-halo. To reject the beam halo induced EM showers, the ECAL signal in the seed crystal of the photon cluster is required to be within 3 ns of the arrival time expected for particles originating from a collision. The potential signal contribution is extracted from the data via simultaneous fits to the E_T^{γ} distributions in the signal and control regions. Predictions for $Z(\nu\nu) + \gamma$, $W + \gamma$, and the beamhalo backgrounds are varied in the fit. Beam halo is not a major background, but the extraction of its rate requires a fit to the observed distributions in the signal region. The splitting of the signal region can be thought of as a two-bin fit. Collision processes occupy the relative fractions of phase space in the horizontal (H) and vertical (V) signal regions, $C_H = 1/\pi$ and $C_V = \pi\text{-}1/\pi$, respectively.

Figure 16.3 shows the observed p_T^{miss} distribution, where data are found to be consistent with the background predictions, and hence limits are set on the DM production cross section assuming a spin-1 mediator.

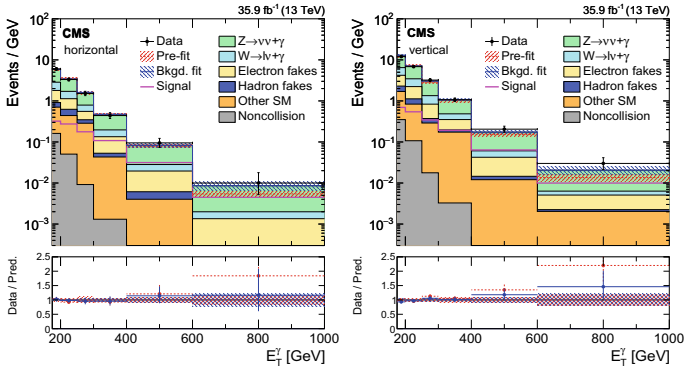

Fig. 16.3 Observed E_T^γ distributions in the horizontal (left) and vertical (right) signal regions compared with the post-fit background expectations for various SM processes. The last bin of the distribution includes all events with $E_T^\gamma > 1000\,\text{GeV}$. The expected background distributions are evaluated after performing a combined fit to the data in all the control samples and the signal region. The ratios of data with the pre-fit background prediction (red dashed) and post-fit background prediction (blue solid) are shown in the lower panels. The bands in the lower panels show the post-fit uncertainty after combining all the systematic uncertainties. The expected signal distribution from a 1 TeV vector mediator decaying to 1 GeV DM particles is overlaid

16.5 MonoHiggs

Due to the fact that the SM Higgs boson couples proportionally to the mass of the particle (Yukawa interaction), an ISR from a initial quark is not the most sensitive way to produce a mono-Higgs signature. In this final state, we consider 2 models Z'2HDM and Baryonic Z'. In Z' 2HDM model, the Z' boson is produced via a quark-antiquark interaction and then decays into a Higgs boson and a pseudoscalar mediator A, which in turn can decay to a pair of Dirac fermion DM particles χ. In Baryonic Z' model, the Z' boson acts as a DM mediator and can radiate a Higgs boson before decaying to a pair of DM particles.

The search is performed in five Higgs boson decay channels [10]: bb, $\gamma\gamma$, ZZ, $\tau\tau$ and WW. The results from the individual channels are combined to obtain the maximum sensitivity. No significant excess over the expected standard model background is observed in any of the five channels or in their combination. Limits are set on DM production in the context of two simplified models. Those channels show a nice complementarity as the bb signature has the largest branching fraction, the diphoton and di-Z signatures have the best resolution on the invariant mass of the Higgs boson and the di-τ channel has the lowest background from SM processes.

The result of the combination is shown in Fig. 16.4 for the Z'-2HDM model. It is clear that the H(bb) channel drives the limit sensitivity on most of the Z' mass range (above 700 GeV) but the other channels become competitive at lower mediator masses.

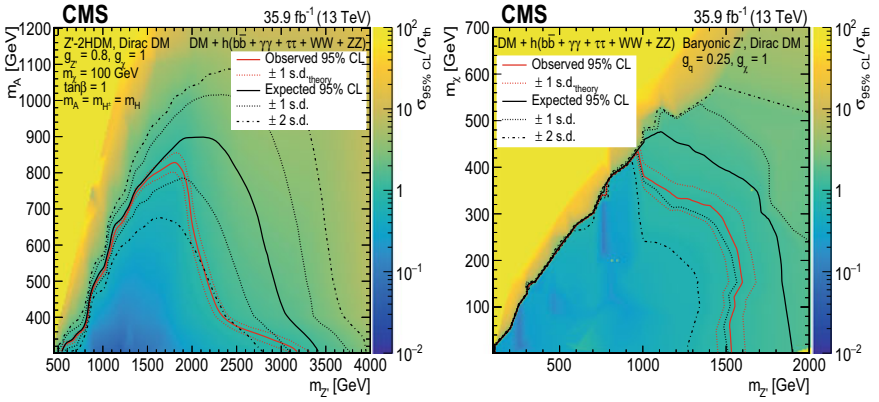

Fig. 16.4 The upper limits at 95% CL on the observed and expected σ/σ_{th} for the Z' 2HDM model (left) and Z'Baryonic model (right)

16.6 Comparison with Direct and Indirect Searches

The limits obtained from the DM searches at the LHC can be translated to limits on the DM-nucleon scattering cross section as measured by their direct detection experiments. Figure 16.5 shows the limits from the mono-Z, mono-jet and mono-γ final state for the vector and axial vector mediator case. The collider limits depend on the choice of the coupling parameters g_q and g_{DM} used in the Simplified model.

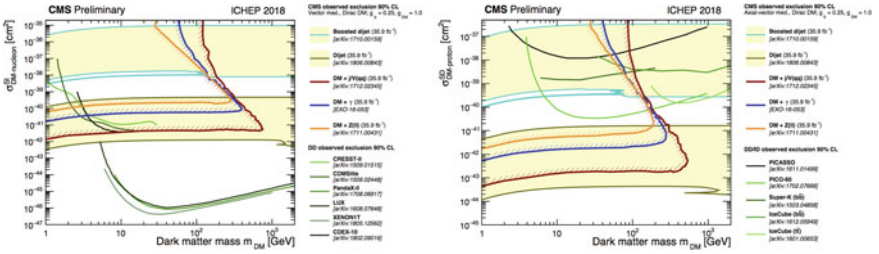

Fig. 16.5 Limits on the spin-independent DM-nucleon scattering cross section from the CMS experiment compared with the results from the direct DM detection experiments (left), and limits on the spin-dependent DM-nucleon scattering cross section from the CMS experiment compared with the results from the direct and indirect DM detection experiments (right). The CMS results are shown assuming a vector mediator and couplings, $g_q = 0.25$, and $g_{DM} = 1.0$

16.7 Summary

The CMS experiment has performed a plethora of dark matter searches [9]. A selection of results based on proton-proton collision data collected in 2016 year has been reported. No significant deviation with respect to standard model predictions have been found and therefore limits on dark matter masses and mediator masses are being set, which are further compared with direct and indirect experiments.

References

1. G. Bertone, D. Hooper, J. Silk, Particle dark matter: evidence, candidates and constraints. Phys. Rept. **405**, 279 (2005). https://doi.org/10.1146/annurev-astro-082708-101659,. arXiv:hep-ph/0404175; J.L. Feng, Dark matter candidates from particle physics and methods of detection, Ann. Rev. Astron. Astrophys. 48 (2010) 495, arXiv:1003.0904; T.A. Porter, R.P. Johnson, P.W. Graham, Dark matter searches with astroparticle data, Ann. Rev. Astron. Astrophys. **49**, 155 (2011). https://doi.org/10.1146/annurev-astro-081710-102528, arXiv:1104.2836. https://doi.org/10.1016/j.physrep.2004.08.031
2. CMS collaboration, The CMS experiment at the CERN LHC, JINT **3** S08004 (2008)
3. C.M.S. Collaboration, Particle-flow reconstruction and global event description with the CMS detector. JINST **12**, P10003 (2017). https://doi.org/10.1088/1748-0221/12/10/P10003. arXiv:1706.04965
4. O. Buchmueller, M.J. Dolan, C. McCabe, Beyond effective field theory for dark matter searches at the LHC. JHEP **01**, 025 (2014). https://doi.org/10.1103/PhysRevD.79.075020. arXiv:1308.6799; Y. Bai, J. Berger, Fermion portal dark matter, JHEP **11**, 171 (2013), arXiv:1308.0612; R. Allahverdi, B. Dutta, Natural GeV dark matter and the baryon-dark matter coincidence puzzle, Phys. Rev. D **88**, 023525 (2013), arXiv:1304.0711; J. Alwall, P. Schuster, N. Toro, Simplified models for a first characterization of new physics at the LHC, Phys. Rev. D **79**, 075020 (2009), arXiv:0810.3921
5. Planck Collaboration, Planck 2015 results. XIII. Cosmological parameters, Astron. Astrophys. **594**, A13 (2016). https://doi.org/10.1051/0004-6361/201525830, arXiv:1502.01589
6. T. Junk, Confidence level computation for combining searches with small statistics. Nucl. Instrum. Meth. A **434**, 435 (1999). https://doi.org/10.1088/0954-3899/28/10/313. arXiv:hep-ex/9902006; A. L. Read, Presentation of search results: the CLs technique, J. Phys. G 28 (2002) 2693, doi: 10.1016/S0168-9002(99)00498-2
7. G. Cowan, K. Cranmer, E. Gross, O. Vitells, Asymptotic formulae for likelihood-based tests of new physics. Eur. Phys. J. C **71**, 1554 (2011). https://doi.org/10.1140/epjc/s10052-013-2501-z]. arXiv:1007.1727. [Erratum: doi: 10.1140/epjc/s10052-011-1554-0
8. C.M.S. Collaboration, Search for new physics in final states with a single photon plus missing transverse momentum in proton-proton collisions at 13 TeV using 2016 data. JHEP **1902**, 074 (2019)
9. http://cms-results.web.cern.ch/cms-results/public-results/publications
10. CMS Collaboration, Search for dark matter particles produced in association with the Higgs boson in proton-proton collisions at 13 TeV, CMS-PAS-EXO-18-011